Materials Today Bio 31 (2025) 101494

Contents lists available at ScienceDirect

Materials Today Bio

journal homepage: www.journals.elsevier.com/materials-today-bio

Biphasic biomimetic scaffolds based on a regionally decalcified bone framework and pre-chondrogenic microspheres for osteochondral defect repair

Zhuo Liang [a,1], Qingqing Pan [a,1], Fei Xue [a,1], Jingdi Zhang [a], Zhenlin Fan [a], Weiyun Wang [a], Xueqiang Guo [a], Zhuang Qian [a], Yaping Shen [a], Wenjuan Song [a], Lei Wang [a], Guangdong Zhou [b,**], Yong He [c,*], Wenjie Ren [a,***]

[a] Clinical Medical Center of Tissue Engineering and Regeneration, The First Affiliated Hospital of Xinxiang Medical University, The Third Affiliated Hospital of Xinxiang Medical University, Institutes of Health Central Plain, Xinxiang Medical University, Xinxiang, 453003, China
[b] Department of Plastic and Reconstructive Surgery, Shanghai 9th People's Hospital, Shanghai Key Laboratory of Tissue Engineering, Shanghai Jiao Tong University School of Medicine, Shanghai, 200011, China
[c] The Second Affiliated Hospital of Zhejiang University and Key Laboratory of 3D Printing Process and Equipment of Zhejiang Province, School of Mechanical Engineering, Zhejiang University, Hangzhou, 310027, China

ARTICLE INFO

Keywords:
Biphasic biomimetic scaffolds
Endochondral ossification
Osteochondral repair
Pre-chondrogenic microspheres
Axitinib

ABSTRACT

Osteochondral defects are still facing a significant challenge in clinical surgery, making post-trauma repair difficult. Tissue engineering has provided a promising approach to solving these defects. However, existing scaffolds cannot replicate the complex biphasic cartilage-bone microenvironment with accuracy. We aimed to develop a biphasic biomimetic scaffold with regionally regulated vascularization that promoted chondrogenesis and osteogenesis through bidirectional regulation of endochondral ossification. This scaffold consisted of pre-chondrogenic microspheres (PCMs) and a decalcified bone frame prepared by decalcifying the cartilage layer and bone layer of the scaffold to varying degrees. Incorporation of PCMs into the cartilage layer created a microenvironment that promoted cartilage regeneration while axitinib was modified to inhibit vascularization and enhance cartilage regeneration. The bone layer provided a microenvironment that promoted endochondral ossification and facilitated bone repair. *In vitro* studies have shown that axitinib-modified cartilage layers significantly inhibit the VEGF expression of pre-chondrogenic cells, while decalcified bone powder from the bone layer significantly promotes the ossification of PCMs. *In vivo* experiments indicated that this decalcified bone frame controls the endochondral ossification of PCMs through regionalized angiogenesis, promoting the integrated regeneration and reconstruction of osteochondral defects in rabbit knee joints. These results suggest that our designed demineralized bone frame can precisely engineer the osteochondral regeneration microenvironment, providing theoretical guidance for the integrated regeneration and repair of anisotropic tissue injuries.

1. Introduction

Osteoarthritis (OA) is a chronic degenerative disease that often involves both the articular cartilage and subchondral bone [1–4]. Articular cartilage has a limited capacity for self-repair *in vivo* and effective repair of articular cartilage defects post-injury has been challenging in clinical surgery [5–10]. Tissue engineering strategies are promising approaches for treating osteochondral defects. Among them, multi-layered biomimetic scaffolds have achieved encouraging results in the regeneration of osteochondral tissues [11,12]. Additionally, tissue engineering strategies based on bone marrow mesenchymal stem cells (BMSCs) are considered an ideal treatment for osteochondral defects [13–15]. Endochondral ossification is an important strategy for bone tissue repair in which BMSCs, after being induced to differentiate into

* Corresponding author.
** Corresponding author.
*** Corresponding author.
E-mail addresses: guangdongzhou@126.com (G. Zhou), yongqin@zju.edu.cn (Y. He), wjren1966@163.com (W. Ren).
[1] These authors contributed equally to this work.

https://doi.org/10.1016/j.mtbio.2025.101494
Received 6 November 2024; Received in revised form 30 December 2024; Accepted 12 January 2025
Available online 13 January 2025

chondrocytes *in vitro*, promote bone injury repair through endochondral ossification *in vivo* [16–19]. Acceleration of the progression of endochondral ossification promotes bone regeneration [18,20]. Inhibiting vascular formation during cartilage regeneration can suppress ossification and contribute to the regeneration of more stable cartilage [21]. Therefore, the design of a biomimetic scaffold that can locally regulate vascular formation in combination with pre-chondrogenic BMSCs is likely to facilitate the integrated regeneration of both cartilage and bone. Previously, we designed a hydrogel microsphere osteogenesis induction system as a bone regeneration unit and combined it with a decalcified bone framework to achieve satisfactory long bone repair in rabbit femoral defects [22]. Based on this strategy, we hypothesized that pre-chondrified hydrogel microspheres would achieve integrated regeneration of cartilage and bone through modulating the biphasic differentiation of endochondral ossification.

Decalcified bone matrix (DBM) has become a promising scaffold for bone repair due to its natural cancellous bone structure, low immunogenicity, good biocompatibility, and tunable mechanical properties [23–26]. Additionally, a combination of the DBM as a framework material and engineered cartilage gel has shown promise for repairing cartilage defects in animals [27]. Therefore, DBM scaffolds with adjustable matrix stiffness appear promising for the development of biomimetic scaffolds that mimic the microenvironment of natural osteochondral bone. An integrated stratified DBM scaffold with different stiffness levels prepared through a controlled paraffin layer embedding has been shown to simulate the mechanical properties of articular cartilage [23,28,29]. Therefore, we hypothesized that paraffin layer embedding could be utilized to achieve layered modification of vascularization inhibitors on the DBM scaffold, thereby enabling localized regulation of vascular formation.

Axitinib acts as a tyrosine kinase inhibitor which can block vascular endothelial growth factor receptor (VEGFR)-mediated endothelial cell migration and growth, induces early endothelial cell apoptosis, prevents vascularization, and inhibits cancer cell growth and invasion through targeting VEGF receptors [30,31]. Research has shown that axitinib facilitates regeneration of stable cartilage in the body [32,33]. Therefore, loading axitinib into the cartilage layer of a biphasic biomimetic scaffold could be considered potentially effective. However, simply adsorbing the drug onto the surface of the DBM scaffold would likely result in low drug-carrying efficiency and sudden release. To address this issue, the surface of the DBM was modified with polydopamine (PDA) to increase the carrying capacity of axitinib. PDA, with its highly reactive catechol groups, can form strong bonds with various material surfaces and facilitate the secondary modification of substrates through interactions with other molecules [34–37]. This approach could enable the preparation of a biphasic biomimetic scaffold that synergistically regenerated the cartilage and subchondral bone, inhibited vascularization in the cartilage layer, and promoted ossification in the bone layer.

In this research, we aim to develop a novel approach for the treatment of full-thickness articular cartilage defects using a biphasic biomimetic scaffold based on a decalcified bone framework and pre-chondrogenic microspheres (PCMs) (Scheme 1). A biphasic DBM scaffold with regional differences in matrix stiffness was created through a stratified decalcification, while a biphasic biomimetic scaffold with regionalized vascular regulation was prepared through modifying the upper layer of the scaffold with axitinib and combining it with PCMs to achieve osteochondral defect repair. In addition, a biphasic biomimetic scaffold loaded with PCMs can enable subcutaneous ectopic cartilage and bone regeneration in nude mice. The full-thickness osteochondral defect model of a rabbit knee joint was then repaired using a biphasic biomimetic scaffold, which showed a satisfactory treatment effect.

2. Materials and methods

2.1. Materials and animals

Gelatin, methacrylic anhydride, and phenyl-2,4,6-trimethylbenzoylphosphonate (LAP) were purchased from Sigma-Aldrich. Insulin-transferrin-sodium selenite was purchased from ScienCell. The microfluidic devices and chips were purchased from Shanghai Pengzan, China. All chemicals are reagent grade and prepared using deionized water. In addition, nude mice and New Zealand white rabbits (2.5–3.0 kg) were supplied and reared by Shanghai Yunde Experimental Animal Raising Farm (Shanghai, China). All animal experimental

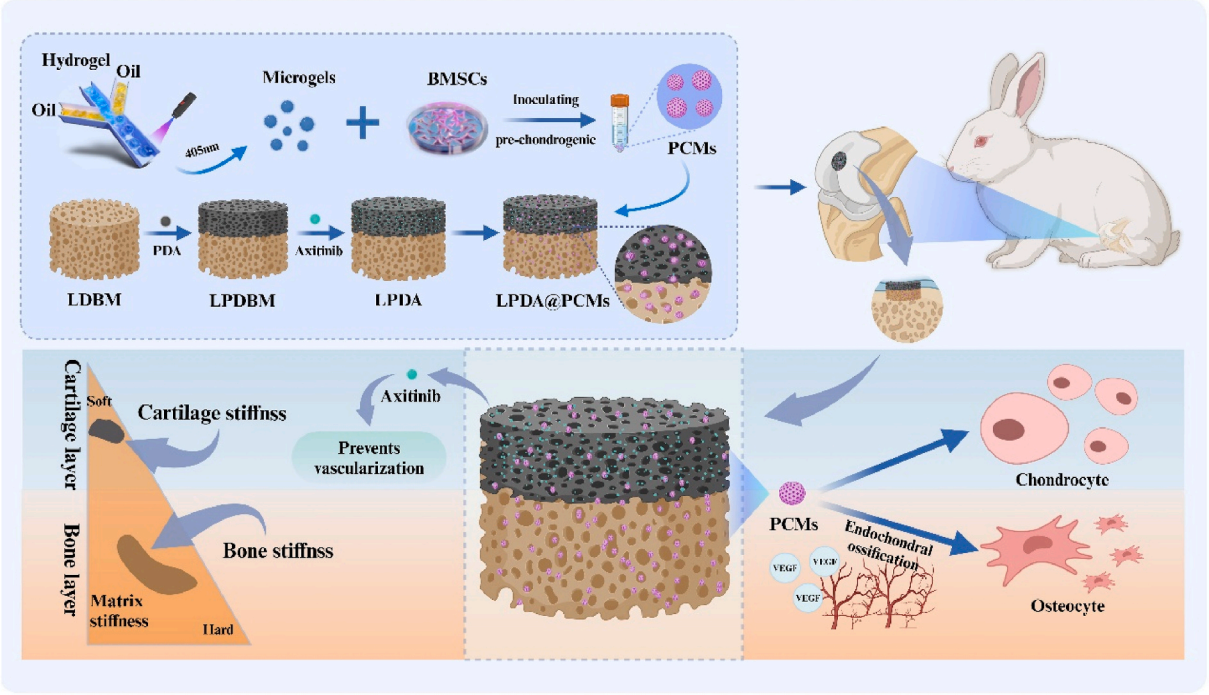

Scheme 1. Schematic diagram of the biphasic biomimetic scaffold based on DBM frame and PCMs for full-thickness osteochondral defects.

methods performed have been approved by the Animal Research Committee of Xinxiang Medical University (Xinxiang, China) (License number: XYLL-20230329).

2.2. Gelatin methacryloyl (GelMA) synthesis

GelMA was synthesized using methacryloyl-modified gelatin, as previously described [38]. Weigh 20 g of gelatin and dissolve it in 200 mL of phosphate-buffered saline (PBS) solution (pH, 7.4) and then stir at 60 °C using a magnetic stirrer. Then, the methacrylate anhydride solution (16 mL) was slowly added dropwise, and the reaction continued for 2 h after the dropwise addition was completed. Finally, the solution was collected and dialyzed in a dialysis membrane (8000-14000 KDa) at 37 °C for 7 d. GelMA is obtained after freeze-drying.

2.3. GelMA microspheres production

GelMA microspheres were prepared as per previous methods [22,39,40]. Briefly, 1 g of GelMA and 25 mg of the LAP photoinitiator were dissolved in 10 mL of PBS solution. The solution was dissolved at 60 °C for 30 min in the dispersed phase (water phase). In addition, 10 mL of droplet-generating oil was used in the oil phase. A microfluidic pump is used to inject the two liquids separately into the channels of the chip, and the aqueous phase is sheared to form microspheres by the shearing action of the oil phase. By manipulating the velocity of the aqueous and oil phases, it is possible to obtain hydrogel microspheres with controlled size. The microspheres were collected in a 15 mL centrifuge tube. The collected droplets are solidified by a UV flashlight (405 nm, 20 mW/cm^2) for 30 s and then polymerized into stable microspheres. The size of the resultant microspheres was determined using microscope images and NIH ImageJ software. The microspheres were first treated with a demulsifying agent, followed by three successive rinses with distilled water, and ultimately lyophilized for later use.

2.4. Characterization of GelMA microspheres

The morphology and structure of GelMA microspheres were detected by scanning electron microscopy (ZEISS Gemini 300). Prior to observation, all samples were sprayed with gold for 60 s (Oxford Quorum SC7620).

Mechanical tests on the GelMA microspheres were performed using a universal material-testing machine (Shimadzu AGS-X-50N, Japan). A compression test was performed at a speed of 1 mm/min, and the elastic modulus was calculated using the resulting stress-strain curve, which was defined as the slope of the linear region at 5%–10 % strain. The modulus of elasticity was calculated as the average of three measurements.

2.5. In vitro GelMA microspheres degradation

For the *in vitro* degradation experiment, 1 mg of the lyophilized microsphere sample was placed in 1 mL PBS solution (pH 7.4) containing 5 U/mL collagenase. In the dry state, the initial weight of the sample was W_0. Lyophilized microspheres were incubated for one week in a shaker at 37 °C. The collagenase solution in the tube was changed daily to ensure a constant concentration, a sample was removed every 24 h to remove the supernatant liquid, and the sample was washed three times with deionized water and then lyophilized, until the weight was W_1.

$$\text{Degradation ratio} = W_1/W_0 \times 100\%$$

2.6. PCMs preparation and biocompatibility

2.6.1. PCMs preparation

BMSCs were obtained from adult rabbit bone marrow blood and cultured and expanded in a 37 °C 5 % CO_2 incubator. The medium was changed every 3 d for use when the cells were expanded to the second generation.

BMSCs of 20 mil/mL were mixed with lyophilized microspheres, placed in ultra-low adhesion 6-well plates, and incubated at 37 °C for 6 h to allow the cells to spread fully on the microspheres surface. After 48 h of amplification and culture, cartilage induction medium was added, and the culture was continued for 28 d to obtain PCMs. The culture was stored in a 37 °C 5 % CO_2 incubator and the medium was changed every 2 d to ensure adequate nutrient supply to the cells.

2.6.2. Cell viability of PCMs

Cell viability was assayed after 1, 7, 14, and 28 d of *in vitro* co-culture, and survival was quantified. As previously described [22], cell viability was assayed using the Calcein-AM/PI Double Staining Kit (DOJINDO, C542, Japan). Specifically, 4 μL of calcein-AM and 6 μL of PI were first added to 2 mL of PBS to prepare a live/dead dye working solution. Approximately 20 mg of PCMs was then added to 2 mL of live/dead dye working solution for live/dead staining, followed by a 15 min incubation at 37 °C protected from light. Photographs were taken using a laser confocal microscope and the number of live and dead cells was quantified by NIH ImageJ software, and finally the ratio of the number of live cells to the total number of cells was calculated to assess cell viability.

2.6.3. Cell spreading of PCMs

Cell adhesion and spreading were measured at 1, 7, 14, and 28 d of *in vitro* co-culture, respectively. F-actin and nuclei were stained with phalloidin and 4′,6-diamidino-2-phenylindole (DAPI) staining solution, respectively. First, after three gentle rinses with PBS solution, fix with 4 % paraformaldehyde solution for 15 min. The sample is permeabilized using a 0.5 % Triton X-100 solution for a duration of 5 min at ambient temperature. After washing with PBS, add 5 μg/mL phalloidin dropwise and incubate for approximately 1 h. The samples were then stained with DAPI staining solution (1:1000 dilution) for nuclei. Finally, images were taken by a laser confocal microscope and the number of cells was measured by NIH ImageJ software.

2.6.4. Pre-chondrogenic differentiation

To prepare PCMs, cell-carrying microspheres were co-cultured in a chondrogenic induction culture medium for 4 w. The expression of cartilage-related genes in the PCMs was assayed using real-time quantitative PCR (RT-qPCR) at 1, 14, and 28 d after chondrogenic induction. In addition, cartilage-induced chondrocyte-associated protein expression in the PCMs at 28 d was detected using immunofluorescence staining.

2.7. Preparation and characterization of biphasic biomimetic DBM scaffolds

2.7.1. Preparation of biphasic biomimetic DBM scaffolds

Fresh pork femurs were purchased from a local slaughterhouse. As previously study, the head of the femur was cut using a saw blade and soaked in a normal saline solution [23]. The femoral head was divided into cylinders 5 mm in diameter and 6 mm thick for the cell and subcutaneous implantation experiments. The cancellous bone was cut into cylinders (diameter, 4 mm; thickness, 4 mm) for the repair of osteochondral defects in the rabbit knee joint. The process of decellularization and degreasing was carried out utilizing Triton X-100 and methanol, respectively. Since the shape and size of the decalcified bone scaffold can be artificially controlled, we used a scaffold with an upper layer of 2 mm and a lower layer of 4 mm in cell experiments and subcutaneous

experiments in nude mice. In animal experiments, the upper layer of our scaffold was 0.5 mm and the lower layer was 3.5 mm. For example, in the cell experiments, the scaffolds were divided into upper (2 mm) and lower (4 mm) layers, and the lower layer (4 mm) was embedded in paraffin, cooled, and placed in an ethylenediamine tetraacetic acid (EDTA) decalcification solution for 2 d. The scaffolds were cleaned with deionized water and dewaxed using xylene after freeze-drying. Double DBM scaffolds were obtained after treatment for 5 d. All scaffolds were then placed in a decalcification solution for one day to partially decalcify the lower layer. After washing with distilled water and freeze-drying, we obtained a layered DBM (LDBM) scaffold with regional variations in matrix stiffness. Finally, the lower layer of LDBM scaffolds was embedded in paraffin. However, the wax-sealed lower scaffold was not loaded with axitinib as it could not be modified via the PDA surface. The upper layer was immersed in 1 mg/mL PDA solution for 24 h to obtained LDBM@PDA (LPD) scaffold. Following washing with distilled water, we obtained a biphasic scaffold with PDA modification on the upper layer and no modification on the lower layer. The scaffold was soaked in 0.16 mg/mL axitinib solution, and xylene was subsequently dewaxed to obtain biphasic biomimetic LPD@Axitinib (LPDA) scaffolds. Finally, xylene was washed with distilled water and freeze-dried to obtain a biphasic bionic scaffold.

2.7.2. Characterization of biphasic biomimetic LPDA scaffolds

The degree of decalcification and stratification of the biphasic biomimetic DBM scaffolds was measured using micro-computed tomography (Micro-CT, PINGSENG Healthcare, VENUS 001) to enable quantification of the bone density in the upper and lower layers of the scaffolds.

Scanning electron microscopy was used to detect the internal pore structure of the scaffold after 60 s of gold spray treatment. The pore size of the scaffold was measured using NIH ImageJ software.

A universal testing machine (Shimadzu AGS-X-50N, Japan) was used to detect and determine the mechanical properties of the scaffold, which was decalcified for 1 d (lower layer of the scaffold) and 3 d (upper layer of the scaffold). Prior to testing, the scaffolds were soaked overnight in PBS. The upper pressure plate was lowered at a compression speed of 1 mm/min to measure the compression modulus. The modulus of elasticity was obtained in a range of 2–5% of the stress-strain curve.

2.7.3. Biocompatibility of the biphasic biomimetic LPDA scaffold

The viability of the BMSCs in the biphasic biomimetic scaffold was assessed using live/dead staining. Five d after inoculation of BMSCs on the scaffold, the scaffold was removed and washed three times with PBS to determine cell viability using a Calcein-AM/PI Double Stain Kit (DOJINDO, C542, Japan). After adding the working solution, the scaffold was incubated at 37 °C for 15 min and then observed, with images taken using confocal microscopy (Leica, DMi8, Germany).

The proliferation of BMSCs in the biphasic biomimetic scaffold was evaluated using a cell counting kit-8 (CCK-8) (Beyotime, C0038, China). A 96-well plate was used for this experiment with a cell count of 2000 cells per well. After co-incubating BMSCs with the extract of the scaffold for 1, 3, and 5 d, the original medium was aspirated and a 10 % CCK-8 working solution was added for incubation at 37 °C for 1.5 h. We then measured the absorbance value at 450 nm with a microplate instrument (Synergy H1, BioTek).

2.7.4. Functional assessment of the biphasic biomimetic DBM scaffold in vitro

To further evaluate the *in vitro* functionality of the biphasic biomimetic scaffold, hydrogel microspheres loaded with BMSCs were subjected to pre-chondrogenic induction for 4 w, followed by the detection of cartilage-related gene expression (*SOX9*, *COL2* and *ACAN*). After co-culturing well-maintained passage 3 (P3) BMSCs with the upper layer of the scaffold for 14 d, the expression level of the vascular endothelial growth factor (*VEGF*) gene was assessed. Additionally, BMSCs subjected to pre-chondrogenic induction for 2 w were switched to a low-glucose complete culture medium supplemented with 0.4 % bone powder and co-cultured for another 14 d, followed by the detection of osteogenesis-related gene expression (*ALP* and *OCN*) (Table S1).

2.8. In vivo implantation of PCMs constructs

We selected nude mice aged 4–6 w (n = 3 per group). Due to the lack of functional T cells in nude mice, they can accept cells, tissues, or tumor transplants from other species (such as humans or rabbits) without triggering significant immune rejection. When rabbit-derived cells are transplanted into nude mice, the absence of T cell functionality prevents the recognition of rabbit cells as "foreign" by the adaptive immune system. This allows the rabbit cells to survive and continue to grow in the nude mouse, providing a suitable model to study the characteristics of rabbit cells or their interactions with the surrounding environment. Subcutaneous injections were administered under sterile conditions. We collected PCMs at a dose of 300 μL and injected them into nude mice subcutaneously using a 1 mL syringe. At 4 and 8 w post-implantation, the samples were fixed with 4 % (w/v) paraformaldehyde solution, ossification of the PCMs was detected using micro-CT, and inflammation and tissue production were detected using histological staining.

2.9. In vivo implantation of the composite biphasic biomimetic LPDA scaffold

Approximately 1 mL of the PCMs was injected into the biphasic biomimetic scaffold for subcutaneous implantation into nude mice after ensuring uniform dispersion. Tissue analysis was performed 4–8 w post-implantation.

2.10. Repair of rabbit articular osteochondral defects

New Zealand white rabbits weighing 2.5–3.0 kg (n = 3 per group) were used, and the experimental method was approved by the Animal Research Committee of Xinxiang Medical University. Eighteen white rabbits were divided into an untreated group (only joint defect surgery), a control group (biphasic biomimetic scaffold implanted after surgery), and an experimental group (PCMs composite biphasic biomimetic scaffold implanted after surgery). Under strict sterile conditions, each rabbit was operated on after general anesthesia, and the knee joint was incised through a medial parapatellar approach. Sterile drilling was used to create full-thickness osteochondral defects (diameter, 4 mm; depth, 4 mm) at the lateral trochlear ridge of the distal femur on both legs. The incision was sutured after surgery was completed, and antibiotics were administered for 3 d after surgery to prevent infection.

2.11. Gross observation and micro-CT analysis

The rabbits were sacrificed 6 and 12 w after surgery to remove the joints and were evaluated by three blinded observers. The International Society for Cartilage Repair (ICRS) Total Scoring System was used to score the degree of repair, integration, surface regularity, and overall condition (Table S2). All samples were fixed with 4 % paraformaldehyde. To assess regeneration of the subchondral bone at 6 w, all samples were scanned and reconstructed using micro-CT. Avatar3 software was used to analyze the ratio of bone volume-to-tissue volume (BV/TV) and trabecular spacing.

2.12. Histological analysis

Joint samples were decalcified in EDTA for 6 and 12 w and then sliced in paraffin for histological analysis. Histology included hematoxylin & eosin (H&E), Masson trichrome (MT), Safflower O and Fast Green staining (SO-FG), as well as immunohistochemical staining of OCN and COL2. Finally, an ICRS score was used to evaluate

osteochondral repair.

2.13. Statistical analysis

All samples and data were presented as mean ± standard deviation (n = 3 per group). Differences between values were evaluated using a one-way analysis of variance (ANOVA) and values of $*p < 0.05$, $**p < 0.01$, $***p < 0.001$, and $****p < 0.0001$ were considered statistically significant.

3. Results

3.1. Microfluidic fabrication and characterization of GelMA microspheres

GelMA microspheres were prepared with water-in-oil emulsification using a microfluidic device. Microspheres prepared using this method had high dispersion and good stability after 30 s of crosslinking with ultraviolet radiation at 405 nm (Fig. 1A and B). Through controlling the velocities of the oil and water phases, we obtained microspheres with an approximate diameter of 115 μm (Fig. 1C). Following crosslinking, the microspheres was washed with a demulsifying agent, washed three times with deionized water, and lyophilized for preservation. The surfaces of the lyophilized spheroids displayed numerous folds that favored cell adhesion and proliferation (Fig. 1D). The particle size profile (Fig. 1E) showed that the microspheres had good monodispersity. To assess the mechanical strength of the GelMA microspheres, their force-displacement curves were measured using a universal testing machine (Fig. 1F). In addition, degradation experiments *in vitro* showed that the spheroids exhibited gradual mass degradation under the influence of *in vitro* collagenase, with complete degradation observed after 6 d (Fig. 1G).

To evaluate the biological activity of the GelMA microspheres, BMSCs and spheroids were co-cultured *in vitro* at a concentration of 20 million cells/mL. Following 1, 7, 14, and 28 d of *in vitro* culture, live/dead and phalloidin staining was performed (Fig. 1H). The results showed that BMSCs displayed high viability throughout the culture

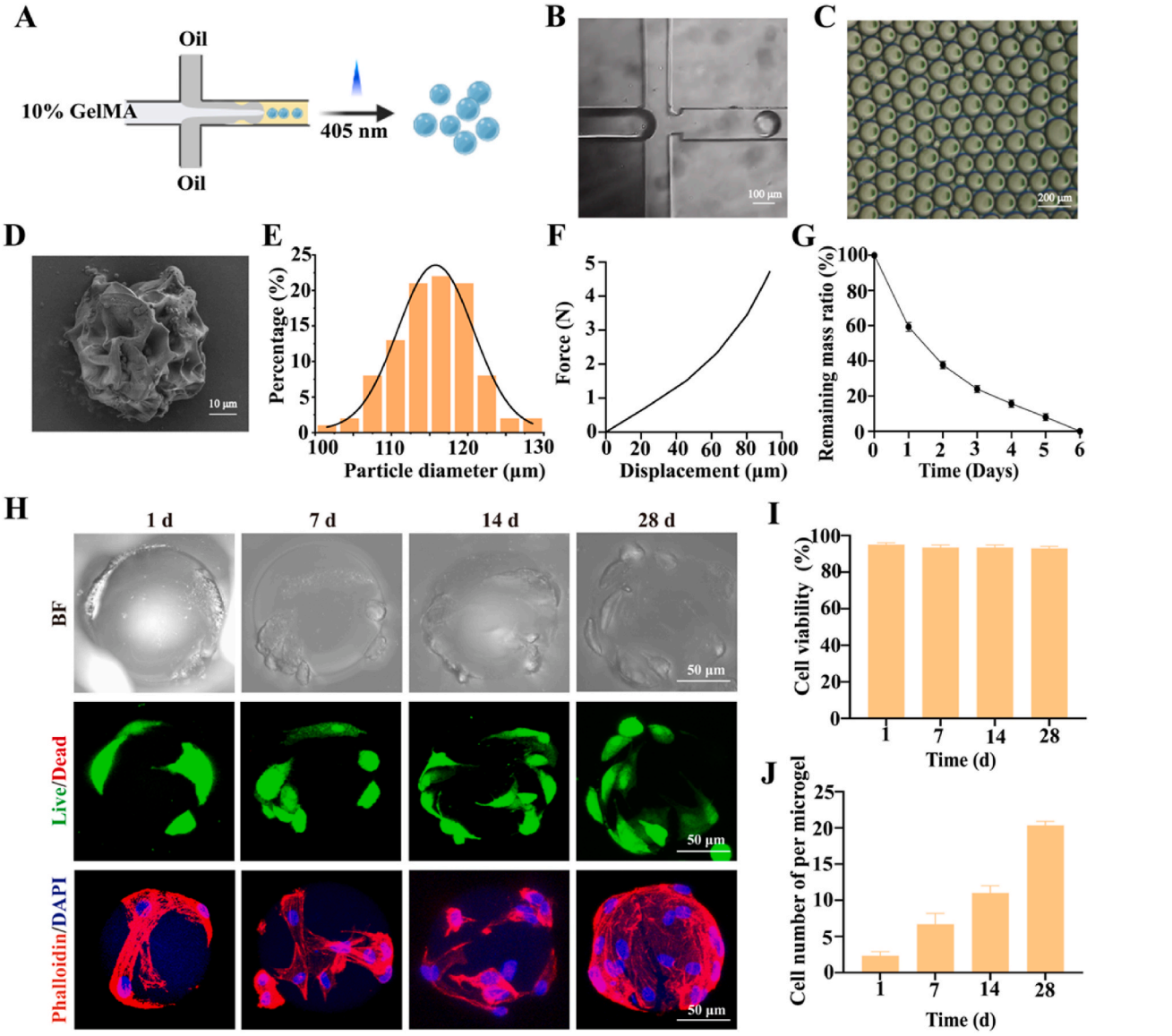

Fig. 1. Fabrication and characterization of GelMA microspheres. A) Schematic diagram of microspheres fabrication. B) Microscope image of the device generating GelMA microspheres. C) GelMA microspheres dispersed in the oil phase under microscopy. D) SEM image of lyophilized microspheres. E) The particle size distribution of GelMA microspheres. F) Force-displacement curve of GelMA microspheres. G) The degradation of GelMA microspheres *in vitro*. H) Live/dead staining and Phalloidin staining during *in vitro* culture at 1, 7, 14, and 28 d. I) Cell viability during *in vitro* co-culture at 1, 7, 14, and 28 d. J) The cell number of per microspheres at 1, 7, 14, and 28 d.

period (Fig. 1I) and exhibited continuous proliferation (Fig. 1J). At 28 d, the cells had covered the entire surface of the microspheres. These findings indicated that microspheres prepared using this method had high dispersion and stability, while facilitating cell adhesion and proliferation. Therefore, these microspheres have the potential to serve as excellent carriers for seed-cell delivery.

3.2. Fabrication and characterization of biphasic biomimetic LPDA scaffolds

Considering the different matrix stiffnesses of cartilage and subchondral bone, scaffold preparation conditions were designed to mimic the mechanical properties of the respective tissues. Micro-CT was used to observe the layered structure of the biphasic scaffolds (Fig. 2A and B). A distinct stratified biphasic scaffold was achieved through selectively decalcifying the scaffold's upper and lower layers to varying degrees;

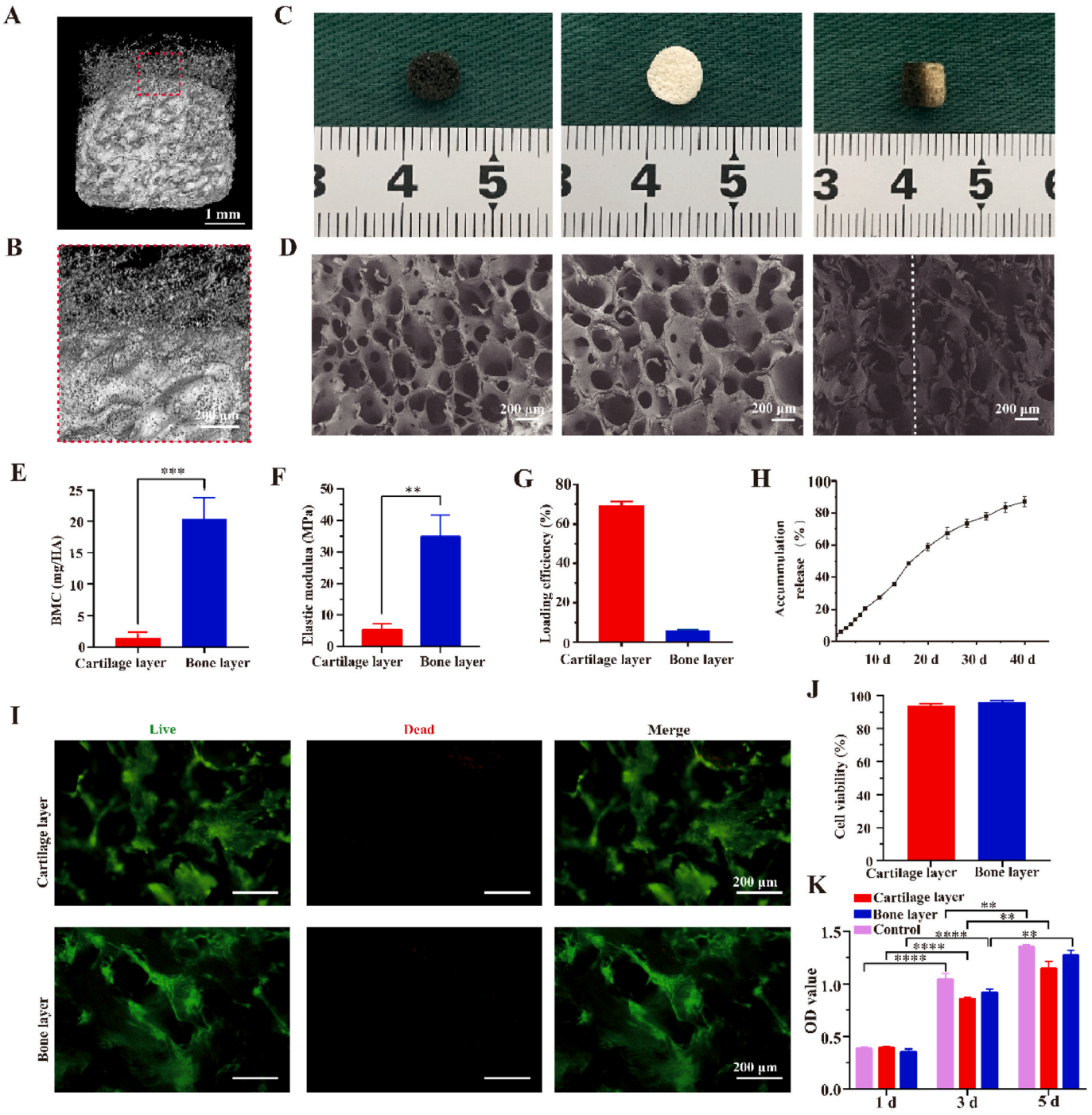

Fig. 2. Fabrication and characterization of the biphasic biomimetic DBM scaffold. A-B) The micro-CT image of the biphasic DBM scaffold. C) The gross view of the biphasic DBM scaffold. D) The SEM image of the biphasic DBM scaffold. E) The BMC analysis of upper and lower layers of the biphasic DBM scaffold. F) Elastic modulus of the biphasic DBM scaffold. G) Loading efficiency of axitinib. H) Cumulative releasing of axitinib from the cartilage scaffolds. I) Live/dead staining after 5 d of co-culture of scaffolds and BMSCs. J) Cell viability after 5 d of co-culture of scaffolds and BMSCs. K) The scaffold extract was incubated for the CCK-8 assay with BMSCs 1, 3, and 5 d.

the lower scaffold exhibited a significantly higher hydroxyapatite content than the upper layer, as quantitatively analyzed (Fig. 2E). Scanning electron microscope results revealed the porous structure of the scaffold (Fig. 2C and D), with the pore size being approximately 300–400 μm. This ensured that GelMA microspheres with a size of 115 μm could be easily injected into the scaffolds without flowing out (Fig. S1). A compression test performed on the scaffold showed that the elastic modulus of the lower layer was significantly higher than that of the upper layer, resembling the characteristics of natural tissue (Fig. 2F). Finally, through surface modification of the upper layer with PDA and electrostatically adsorbed axitinib to maintain the upper scaffold only, a biphasic biomimetic scaffold was achieved. The loading efficiency of axitinib in the PDA modified cartilage layer was significantly higher than that in the bone layer (Fig. 2G). In addition, our findings demonstrated that the cumulative release curve of axitinib from PDA modified cartilage layer lasted for 40 d (Fig. 2H).

BMSCs were cultured to further confirm the biocompatibility of the biphasic biomimetic scaffold. Live/dead staining showed uniform and robust growth of cells in both the upper and lower regions of the scaffold, with a survival rate >95 % and a minimal presence of dead cells (Fig. 2I and J). The CCK-8 assay showed that the cells continued to proliferate with increasing culture time (Fig. 2K).

These results suggest that the layered decalcification- and surface-modification-based biphasic biomimetic scaffold exhibited a porous structure, similar mineral content, and an elastic modulus comparable to those of cartilage and subchondral bone. Moreover, it displayed excellent biocompatibility and provided a suitable microenvironment for repairing osteochondral defects.

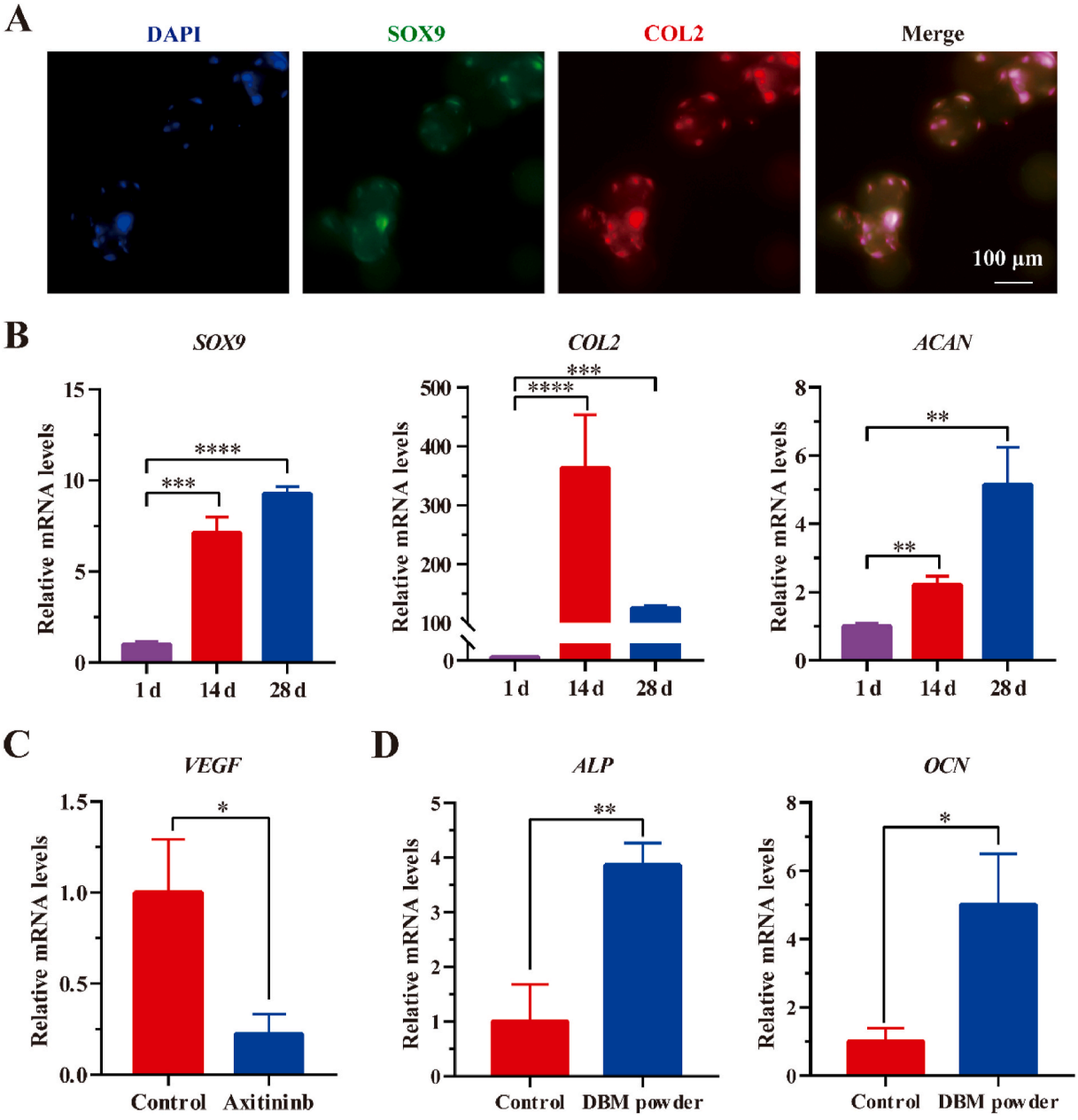

Fig. 3. The biological functional evaluation of PCMs and biphasic biomimetic scaffolds *in vitro*. A) Immunofluorescence staining for cartilage-specific proteins SOX9 and COL2 on microspheres with 28 d of pre-chondrogenic differentiation. B) The qPCR analysis of cartilage-specific genes SOX9, COL2, and ACAN was performed on microspheres after 1, 14, and 28 d of pre-chondrogenic differentiation. C) VEGF expression in pre-chondrogenic BMSCs co-cultured with the upper scaffold for 14 d. D) Osteogenesis-specific genes ALP and OCN were analyzed by qPCR after addition of decalcified bone powder to pre-chondrogenic BMSCs.

3.3. *In vitro biological functional evaluation of PCMs and biphasic biomimetic scaffolds*

It has previously been reported that during endochondral ossification, mesenchymal stem cells differentiate into a callus, which eventually hypertrophies and calcifies [17]. In our study, we obtained PCMs after the pre-chondrogenic induction of GelMA microspheres loaded with BMSCs for 28 d. Through adding different inducing factors to PCMs, we achieved bidirectional differentiation toward both bone and cartilage. During pre-chondrogenic induction, the expression of

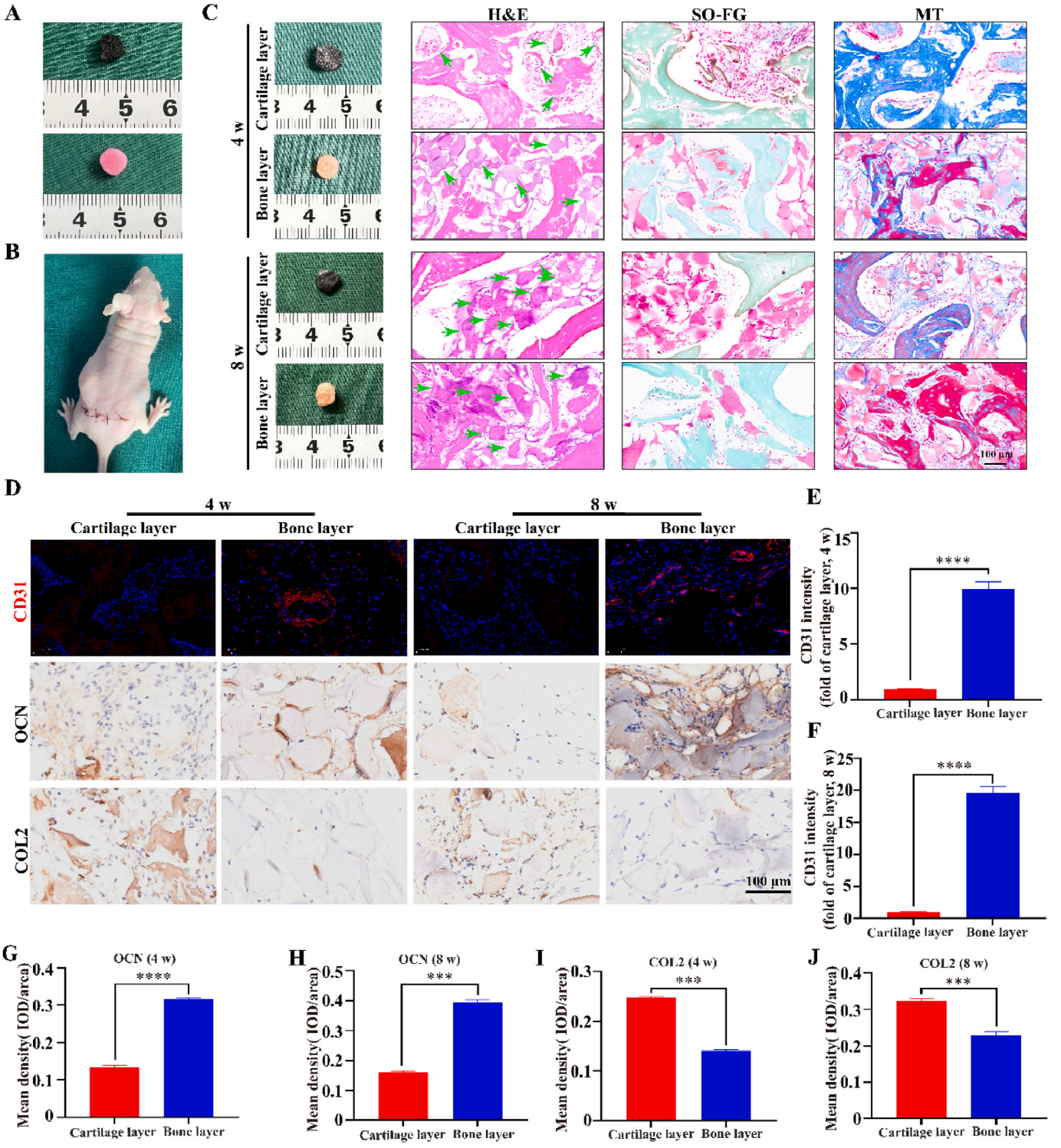

Fig. 4. The biphasic biomimetic scaffold loaded with PCMs can promote cartilage and bone regeneration *in vivo*. A, B) General view and subcutaneous implantation of PCMs-loaded biphasic biomimetic DBM scaffold. C) Gross observation and histological staining of H&E, SO-FG, and MT staining after 4 and 8 w of implantation. The green arrow indicates PCMs. D) Immunofluorescence staining of CD31 and immunohistochemical staining of OCN and COL2 after 4 and 8 w of implantation. E,F) Representative images of the fluorescence intensity of CD31 after 4 and 8 w of implantation. G,H) Quantification of the immunohistochemical staning of OCN after 4 w and 8 w of implantation. I,J) Quantification of the immunohistochemical staning of COL2 after 4 w and 8 w of implantation. (For interpretation of the references to colour in this figure legend, the reader is referred to the Web version of this article.)

cartilage-related genes (SOX9, COL2, and ACAN) was analyzed. Strong gene expression was observed in PCMs (Fig. 3A and B). Additionally, RT-qPCR results showed significant upregulation of cartilage-related genes at 14 and 28 d of induction compared with that at 1 d of induction, indicating successful *in vitro* preparation of PCMs.

Subsequently, we verified the *in vitro* biological functions of the biphasic biomimetic scaffolds. BMSCs were induced in the upper scaffold for 14 d following pro-chondrogenic induction to investigate the inhibitory effects of axitinib on vascularization *in vitro*. Simultaneously, decalcified bone powder was added to the BMSCs after pre-chondrogenic induction to verify whether the lower scaffold promoted bone formation *in vitro*. The qPCR results in Fig. 3C show that the use of Axitinib after pre-chondrogenic induction effectively inhibited the expression of the vascular-associated gene *VEGF*. Moreover, the expression of the osteogenesis-specific genes *ALP* and *OCN* significantly increased after the addition of decalcified bone powder (Fig. 3D). This can be attributed to the minerals present in the decalcified bone powder as well as the presence of calcium and phosphate ions, which promote the differentiation of pre-chondrogenic stem cells toward bone formation. In summary, the biphasic biomimetic scaffold provided a favorable microenvironment for cartilage and bone regeneration and differentiation *in vitro*.

3.4. Subcutaneous cartilage ossification of PCMs

To verify the cartilage and endochondral bone regeneration potential of the PCMs *in vivo*, we injected 300 μL of PCMs into the subcutaneous tissue of nude mice, as depicted in Fig. S2A. Gross and micro-CT evaluations at 4 w post-implantation revealed ossification, with most of the tissue retaining a cartilage-like appearance. At 8 w post-implantation, increased bone formation was observed (Fig. S2B). These results suggest that bone regeneration can be achieved through endochondral ossification, and they provide favorable evidence that the cartilage layer may be vascularized. Quantitative analysis of bone volume (mm^3) and BV/TV (%) was consistent with the above results (Figs. S2C and D). Histological examination further confirmed that PCMs cultured produced slight vascularization and small bone regeneration after 4 w of subcutaneous injection. At 8 w, the PCMs exhibited relatively mature vascularization and ossification (Fig. S2E, F and G). These results suggest that PCMs in the subcutaneous environment are vascularized and ossified, making it challenging to maintain stable cartilage regeneration. This finding further supports the inclusion of axitinib in biphasic biomimetic scaffolds.

3.5. Biphasic biomimetic DBM scaffolds loaded with PCMs implanted subcutaneously in vivo to promote the synergistic differentiation of cartilage and osteogenesis

The cartilage layer and bone layer of the biphasic biomimetic scaffold loaded with PCMs were implanted subcutaneously into nude mice to evaluate their ability to promote synergistic cartilage and bone regeneration. The PCMs were uniformly injected into the scaffold, which was then buried in the back skin of the nude mice (Fig. 4A and B). After 4 and 8 w of implantation, both the cartilage layer and bone layer of the scaffold still retained the original size and shape, and the scaffold was evenly filled with PCMs. Additionally, the bone layer exhibited the formation of reddish tissue resembling bone (Fig. 4C). Histological staining analysis showed that the cartilage layer maintained the characteristics of the cartilage, as evidenced by the expression of the cartilage-related protein COL2 at 4 and 8 w. The bone layer showed new bone formation, and the new bone tissue was connected to the scaffold to form complete bone tissue (Fig. S3). Additionally, the bone-associated protein OCN was strongly expressed only in the bone layer (Fig. 4D–G and H). The cartilage-associated protein COL2 was strongly expressed only in the cartillage layer (Fig. 4D–I and J) The vascular marker CD31 was expressed only in the bone layer at 4 and 8 w, indicating that axitinib loaded into the cartilage layer effectively inhibited vascularization, thereby promoting cartilage development (Fig. 4D, E and F). These findings indicated that when loaded with PCMs, the biphasic biomimetic scaffold can promote osteochondral regeneration through creating a conducive cartilage microenvironment and an osteogenic microenvironment, while also facilitating the regulation of endochondral ossification.

Furthermore, the biphasic scaffold was implanted subcutaneously in rat to assess its ability to regulate regionalized angiogenesis. After 4 w of subcutaneous implantation, a large number of CD31-positive cells and microvascular were observed in the bone layer region (Fig. S4A). In stark contrast, the cartilage layer region had few CD31-positive marked cells and microvascular structures. At 8 w post-implantation, similar trends were observed in both the bone and cartilage regions (Fig. S4B). The results demonstrate that the stratified modification with axitinib can achieve regionalized angiogenesis regulation in an integrated scaffold.

3.6. Osteochondral repair based on LPDA scaffolds loaded with PCMs

To investigate the effectiveness of biphasic cartilage-bone-integrated tissue regeneration *in vivo*, we used a rabbit knee joint model. Refer to the previous method [41] a cylindrical osteochondral defect (diameter, 4 mm; depth, 4 mm) was created at the trochlea of the rabbit knee using a dental drill, and LPDA loaded with PCMs was implanted (Fig. 5A and B). The untreated group received unfilled scaffolds, whereas the control group received biphasic biomimetic scaffolds without PCMs.

As shown in Fig. 5C, the surgical area remained evident in the untreated group at 6 w, with fibrous tissue repair becoming visible at 12 w. The control group exhibited some fibrous tissue repair at 6 w, and the defect area was significantly reduced at 12 w, with a small amount of cartilage-like tissue forming at the edges.

Micro-CT results indicated that the bone defect area was partially repaired by the scaffold in the control group; however, a large number of defects were still visible in the center at 6 w (Fig. 5D). In the experimental group, a substantial amount of newly formed cartilage-like tissue was shown in the cartilage defect area at 6 and 12 w, and bone defect area exhibited satisfactory regeneration. Both the cartilage and bone defects were effectively repaired. At 6 w, the surface of the cartilage defect area appeared relatively rough and incomplete; however, at 12 w, the defect area had a relatively smooth surface, indicating better chondrogenesis.

Quantitative analysis, including ICRS macroscopic scores (BV/TV) and trabecular spacing at 6 w, indicated that the experimental group exhibited excellent cartilage and bone regeneration outcomes (Fig. 5E, F and G). However, there was no significant difference between the control group and the experimental group in terms of bone-related indicators. This may be attributed to blood gushing during surgery in the control group, which provided a small number of BMSCs to sustain bone remodeling.

These observations were proved using histological staining (Fig. 6A). The untreated group mainly showed repair with fibrous tissue at 6 and 12 w, and there were obvious defects in the cartilage and subchondral bone in the defect area. At 12 w, the cartilage layer in the control group mainly showed repair in the cartilage region with both fibrous and cartilaginous tissue, whereas the subchondral bone region was comparatively better repaired than that in the untreated group owing to the filling of the scaffold. Consistent with these general observations, in the experimental group, cartilage-like tissue was regenerated from the cartilage defect area, and at 6 w, a large amount of cartilage layer was observed to be filled and showed smoothness, and a large number of new bone formations were observed in the subchondral bone area. Some defects in the subchondral bone region remained present at 6 w. However, both the cartilage and subchondral bone exhibited robust regeneration with a clear interface between the two tissues at 12 w. Histological examination using H&E, Masson, and SO-FG staining

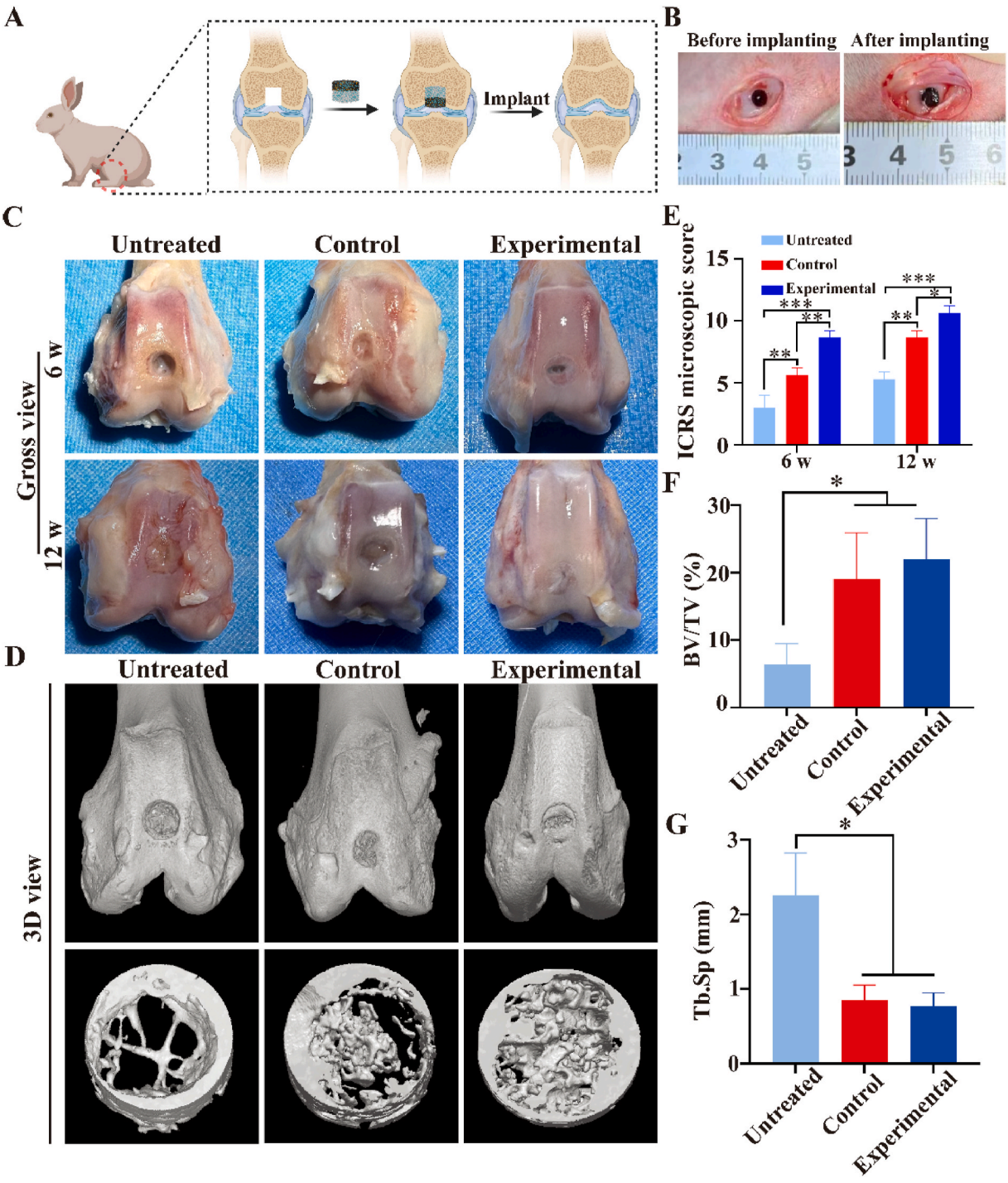

Fig. 5. In vivo repair of osteochondral defects was performed in a rabbit knee model (6 w and 12 w post-surgery). A) A schematic of surgery processes for rabbit knee joint model. B) Gross view of osteochondral defects before and after stent implantation. C) Gross view of the articular cartilage at 6 w and 12 w post-surgery. D) Micro-CT images of the repaired osteochondral defects in each group at 6 w. E) ICRS microscopic scores at 6 w and 12 w for each group were repaired. F, G) The volume ratio of the newly formed bone to the total volume of defect region (BV/TV) and trabecular density (Tb.Sp) analyzed from micro-CT images at 6 w.

revealed an increased number of newly formed cartilage lacunae, with chondrocytes displaying a regular arrangement. Immunohistochemical staining for COL2 and OCN showed positive results (Fig. 6B).

4. Discussion

We developed a novel strategy for a biphasic biomimetic scaffold consisting of a regionally vascularized decalcified bone framework and PCMs with the aim of providing an alternative approach for repairing full-thickness joint defects. Hydrogel microspheres with a diameter of approximately 115 μm were prepared using microfluidics. PCMs were then obtained through pre-chondrogenic induction for 28 d. The biphasic biomimetic scaffold exhibited mineral content and mechanical stiffness similar to those of natural cartilage and subchondral bone. The cartilage scaffold inhibited *VEGF* gene expression in the cartilage regeneration unit, whereas the bone scaffold promoted osteogenic differentiation of the PCMs, providing suitable mechanical support and an optimal induction environment for cartilage and subchondral bone

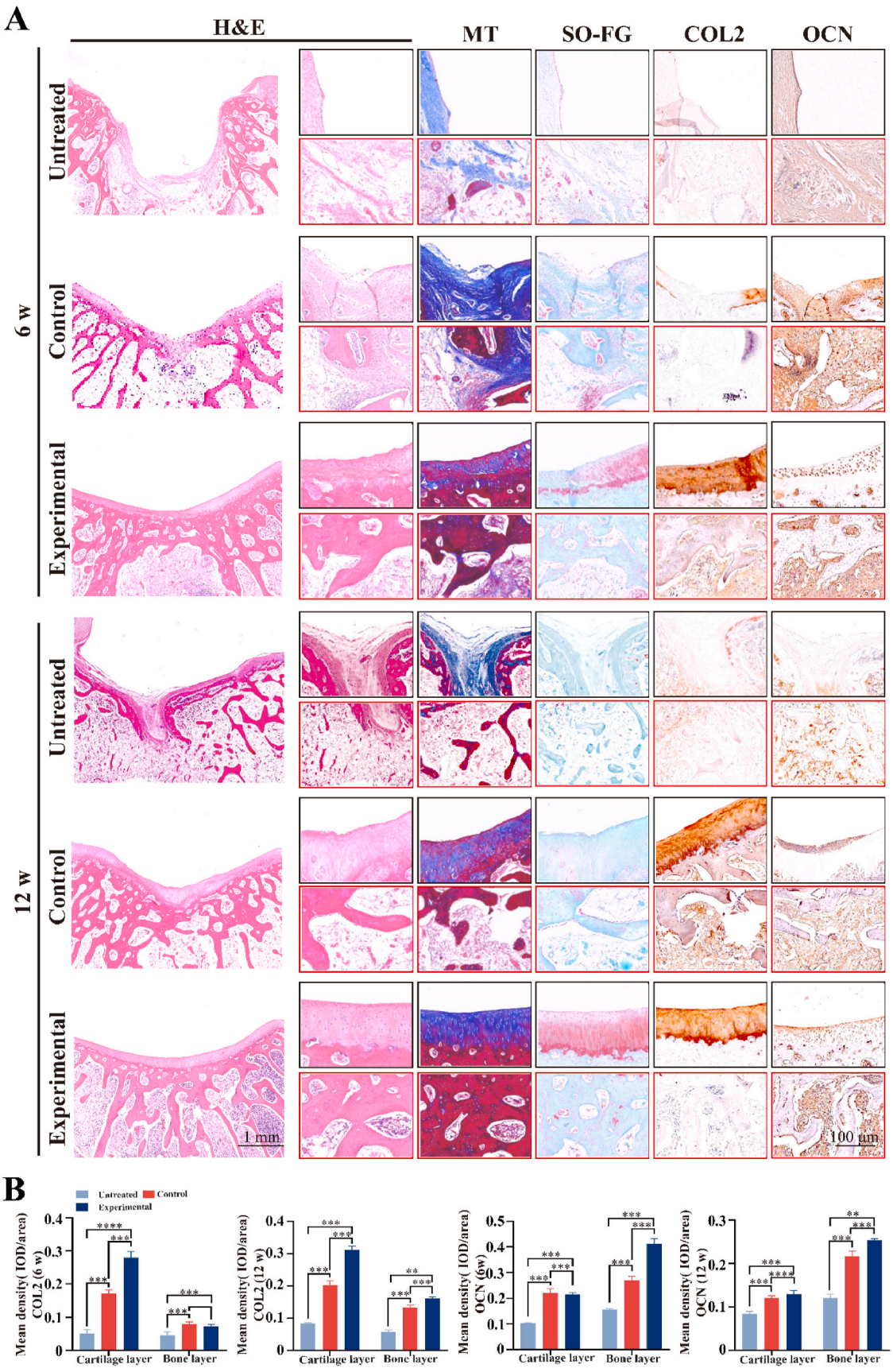

Fig. 6. Histological staining analysis. A) Histological examinations (H&E, MT, SO-FG staining and immunohistochemical staining of OCN and COL2) of samples at 6 w and 12 w post-surgery. B) Quantification of the immunohistochemical staning of OCN and COL2 after 6 and 12 w post-surgery.

regeneration. Through combining PCMs with biphasic biomimetic scaffolds, full-thickness articular cartilage defects were successfully repaired in a rabbit knee joint model, thereby offering a promising alternative to joint bionic repair materials.

Two challenges were encountered during the preparation of PCMs. We first ensured that the sizes of the hydrogel microspheres matched that of the decalcified bone framework. Considering that the decalcified bone frame's size was approximately 300–400 μm, which was too large to be injected into the scaffold's interior, we prepared 115 μm hydrogel microspheres through adjusting the speed of the oil and water phases. *In vitro* experiment findings indicated that these microspheres exhibited good biocompatibility (Fig. 1H), facilitating the long-term culture of cartilage regeneration units. It is also essential to determine the duration of pre-chondrogenic induction for the loaded hydrogel microspheres. If the induction time is too short, the microspheres do not develop a relatively stable cartilage phenotype [42]. Conversely, an excessively long induction time hinders the internal ossification of the cartilage tissue [43,44]. Based on previous studies [17], we selected a 4 w pre-cartilage induction period for subsequent experiments. Immunofluorescence staining and RT-qPCR experiments targeting cartilage-specific proteins confirmed that PCMs induced after 4 w of pre-cartilage induction exhibited relatively mature cartilage characteristics (Fig. 3A and B).

Scaffolds play a significant and essential role in tissue regeneration. Osteochondral tissue is composed of cartilage and subchondral bone. Therefore, it is important to explore new strategies to promote the integrated regeneration of osteochondral tissue. Previous monophasic biomimetic scaffolds have had difficulty providing an ideal microenvironment for osteochondral tissue repair. Moreover, the current widely applied biphasic biomimetic scaffold strategies have shown poor mechanical strength and stratification at the cartilage-subchondral bone interface, failing to promote the integrated repair of bone-cartilage in a way that is both independent and tightly integrated [45,46]. The DBM scaffolds is widely used in cartilage and bone repair owing to its natural cancellous bone structure, good biocompatibility, and low immunogenicity. Completely decalcified DBM has matrix stiffness similar to natural cartilage and diminished osteoinductive potential. However, the DBM, as a matrix material with good bone induction, may cause cartilage differentiation into bone, and it is difficult to obtain stable cartilage regeneration if the surface is not modified. To ensure stable cartilage generation, we loaded the scaffold with axitinib to inhibit vascularization during cartilage repair. The analysis of cellular compatibility indicates that the modified axitinib scaffold still possesses excellent biocompatibility. The RT-qPCR results showed that PCMs co-cultured with axitinib-loaded scaffolds effectively reduced *VEGF* expression (Fig. 3C), thus preventing vascularization during chondrogenesis. Furthermore, the partially decalcified DBM scaffold simulated the matrix stiffness of natural bone tissue and provided high osteoinduction activity, thereby providing a favorable microenvironment for endochondral ossification. Quantitative analysis of osteogenesis-related genes also indicated that the regeneration unit with pre-chondrogenic induction for 4 w promoted bone regeneration through endochondral ossification using the osteoinductive activity of decalcified bone (Fig. 3D). These results suggest that the bone layer scaffold has the potential to induce PCM bone formation.

Following the *in vitro* construction, it was essential to determine whether the composite scaffold loaded with PCMs could regenerate stable cartilage and bone tissues *in vivo*. Subcutaneous implantation results showed that the composite scaffold loaded with PCMs partially regenerated cartilage and bone at 4 w and successfully regenerated stable cartilage and bone structures at 8 w, indicating reliable and stable osteochondral regeneration. Finally, determining whether a composite scaffold loaded with PCMs can achieve integrated joint regeneration *in vivo* is a challenging issue in clinical practice. In the repair and regeneration of osteochondral defects in the rabbit knee joint, both macroscopic observations and pathological staining results demonstrated that the composite biphasic biomimetic scaffold loaded with pre-chondrogenic stem cell microspheres successfully repaired and reconstructed the osteochondral defects at the femoral trochlea. In the experimental group, newly formed chondrocytes appeared at 6 w post-surgery, and over time, by 12 w post-surgery, the chondrocytes matured further. These findings were consistent with the results of H&E, Masson, SO-FG, and COL2 immunohistochemical staining. Additionally, as time progressed, the subchondral bone repair also exhibited significant regenerative effects. These results indicate that our synthesized scaffold, through regional vascular formation regulation and precise control of matrix mechanical properties to modulate the endochondral ossification process of PCMs, achieves bidirectional differentiation control of chondrogenesis and osteogenesis.

Our findings showed that the biphasic biomimetic scaffold without PCMs exhibited a certain degree of regenerative effect in bone regeneration, possibly due to the filling and presence of a substantial amount of blood in the subchondral bone defect area, which provided some seed cell sources and contributed to bone repair [47,48]. Similar to the bone layer, a large amount of blood filling the defect area to some extent promotes cartilage regeneration. The microfracture technique, utilized for addressing injuries in articular cartilage, aims at fostering cartilage regeneration by leveraging mesenchymal stem cells and growth factors derived from the surgical site's blood supply. This process necessitates a substantial quantity of seed cells. However, the release of mesenchymal stem cells from the subchondral bone layer is often limited, and these cells must traverse the subchondral bone to reach the cartilage. Consequently, the cartilage frequently receives an inadequate number of mesenchymal stem cells to facilitate regeneration. In contrast to the control group, PCMs (presumably particulate joint matrix) can offer the requisite seed cells for cartilage regeneration. Moreover, the introduction of blood not only supplies these essential cells but also provides the necessary nutrients to support the regeneration process of PCMs. In addition, the mechanism of axitinib-loaded scaffold inhibiting the vascularization of the cartilage layer is quite important. We have explored and preliminarily studied this mechanism through transcriptome sequencing, and axitinib can inhibit the activity of matrix metalloproteinase MMPs by reasonably regulating the VEGF/TIMP signaling pathway during advanced chondrogenesis, thereby inhibiting vascularization and ultimately maintaining the stability of cartilage phenotype [33]. In contrast, biphasic biomimetic scaffolds loaded with PCMs achieved stable regeneration of both cartilage and continuous bone tissue, indicating that the addition of PCMs significantly improved osteochondral repair outcomes. Additionally, satisfactory articular cartilage repair results can be attributed to the stable microenvironment provided by the biphasic biomimetic scaffold, its appropriate mechanical stiffness, and the abundant cell sources provided by the PCMs.

5. Conclusion

We developed a novel strategy for osteochondral defect repair and successfully constructed a biomimetic scaffold through combining PCMs with biphasic biomimetic scaffolds and achieved reliable cartilage and bone regeneration in a subcutaneous environment. This biphasic biomimetic scaffold containing PCMs was used for full-thickness osteochondral defects in rabbits and satisfactory osteochondral regeneration was achieved. While its effectiveness in large animal models has not yet been investigated, this study provides a promising method for repairing osteochondral defects.

CRediT authorship contribution statement

Zhuo Liang: Writing – original draft, Data curation, Conceptualization. **Qingqing Pan:** Writing – original draft, Formal analysis, Data curation, Conceptualization. **Fei Xue:** Writing – original draft, Formal analysis. **Jingdi Zhang:** Writing – original draft, Methodology. **Zhenlin Fan:** Investigation, Funding acquisition. **Weiyun Wang:** Resources,

Project administration. **Xueqiang Guo:** Validation, Supervision. **Zhuang Qian:** Visualization, Validation. **Yaping Shen:** Resources, Data curation. **Wenjuan Song:** Validation, Supervision. **Lei Wang:** Visualization, Supervision. **Guangdong Zhou:** Writing – review & editing. **Yong He:** Writing – review & editing, Visualization. **Wenjie Ren:** Writing – review & editing, Funding acquisition.

Ethical approval

All animal experimental methods performed have been approved by the Animal Research Committee of Xinxiang Medical University (Xinxiang, China) (License number: XYLL-20230329).

Declaration of competing interest

The authors declare that they have no known competing financial interests or personal relationships that could have appeared to influence the work reported in this paper.

Acknowledgement

This research was supported in part by grants from the Key Research and Development and Promotion Special (Science and Technology) Project of Henan Province (No. 242102230124; No. 242102310321), the Open Research Fund of Tissue Engineering and Regenerative Clinical Medical Center of Xinxiang Medical University (No. 2024YFYKFKT02; No. 2022YFYKFKT05), The Natural Science Foundation of Henan Province (No. 232300421314), the Key Scientific Research Projects of Universities in Henan Province (No. 23B416002; No. 25A430023), the National Natural Science Foundation of China (No. 32200754; No. 82471191; No. 52235007; No. T2121004; No. 52325504), Natural Science Foundation of Henan, China (No. 202300410320), the open project program of the third Affiliated Hospital of Xinxiang Medical University (No. 2022KFKTYB06; No. 2022KFKTYB07; No. 2022KFKTZD03) and the Innovation Support Program of Xinxiang Medical University (YJSCX202265Y).

Appendix A. Supplementary data

Supplementary data to this article can be found online at https://doi.org/10.1016/j.mtbio.2025.101494.

Data availability

The authors do not have permission to share data.

References

[1] J. Martel-Pelletier, A.J. Barr, F.M. Cicuttini, P.G. Conaghan, C. Cooper, M. B. Goldring, S.R. Goldring, G. Jones, A.J. Teichtahl, J.P. Pelletier, Osteoarthritis, Nat. Rev. Dis. Prim. 2 (2016) 16072, https://doi.org/10.1038/nrdp.2016.72.

[2] E.A. Makris, A.H. Gomoll, K.N. Malizos, J.C. Hu, K.A. Athanasiou, Repair and tissue engineering techniques for articular cartilage, Nat. Rev. Rheumatol. 11 (2015) 21–34, https://doi.org/10.1038/nrrheum.2014.157.

[3] Y. Liu, L. Peng, L. Li, C. Huang, K. Shi, X. Meng, P. Wang, M. Wu, L. Li, H. Cao, K. Wu, Q. Zeng, H. Pan, W.W. Lu, L. Qin, C. Ruan, X. Wang, 3D-bioprinted BMSC-laden biomimetic multiphasic scaffolds for efficient repair of osteochondral defects in an osteoarthritic rat model, Biomaterials 279 (2021) 121216, https://doi.org/10.1016/j.biomaterials.2021.121216.

[4] L. Zheng, D. Li, W. Wang, Q. Zhang, X. Zhou, D. Liu, J. Zhang, Z. You, J. Zhang, C. He, Bilayered scaffold prepared from a kartogenin-loaded hydrogel and BMP-2-derived peptide-loaded porous nanofibrous scaffold for osteochondral defect repair, ACS Biomater. Sci. Eng. 5 (2019) 4564–4573, https://doi.org/10.1021/acsbiomaterials.9b00513.

[5] C. Deng, H. Zhu, J. Li, C. Feng, Q. Yao, L. Wang, J. Chang, C. Wu, Bioactive scaffolds for regeneration of cartilage and subchondral bone interface, Theranostics 8 (2018) 1940–1955, https://doi.org/10.7150/thno.23674.

[6] T. Gotterbarm, W. Richter, M. Jung, S. Berardi Vilei, P. Mainil-Varlet, T. Yamashita, S.J. Breusch, An in vivo study of a growth-factor enhanced, cell free, two-layered collagen-tricalcium phosphate in deep osteochondral defects, Biomaterials 27 (2006) 3387–3395, https://doi.org/10.1016/j.biomaterials.2006.01.041.

[7] Y. Hua, Y. Huo, B. Bai, J. Hao, G. Hu, Z. Ci, X. Wu, M. Yu, X. Wang, H. Chen, W. Ren, Y. Zhang, X. Wang, G. Zhou, Fabrication of biphasic cartilage-bone integrated scaffolds based on tissue-specific photo-crosslinkable acellular matrix hydrogels, Mater Today Bio 17 (2022) 100489, https://doi.org/10.1016/j.mtbio.2022.100489.

[8] W. Wei, W. Liu, H. Kang, X. Zhang, R. Yu, J. Liu, K. Huang, Y. Zhang, M. Xie, Y. Hu, H. Dai, A one-stone-two-birds strategy for osteochondral regeneration based on a 3D printable biomimetic scaffold with kartogenin biochemical stimuli gradient, Adv Healthc Mater 12 (2023) e2300108, https://doi.org/10.1002/adhm.202300108.

[9] L. Zhang, W. Dai, C. Gao, W. Wei, R. Huang, X. Zhang, Y. Yu, X. Yang, Q. Cai, Multileveled hierarchical hydrogel with continuous biophysical and biochemical gradients for enhanced repair of full-thickness osteochondral defect, Adv Mater 35 (2023) e2209565, https://doi.org/10.1002/adma.202209565.

[10] C. Aulin, M. Jensen-Waern, S. Ekman, M. Hägglund, T. Engstrand, J. Hilborn, P. Hedenqvist, Cartilage repair of experimentally 11 induced osteochondral defects in New Zealand White rabbits, Lab Anim 47 (2013) 58–65, https://doi.org/10.1177/0023677212473716.

[11] C. Gao, W. Dai, X. Wang, L. Zhang, Y. Wang, Y. Huang, Z. Yuan, X. Zhang, Y. Yu, X. Yang, Q. Cai, Magnesium gradient-based hierarchical scaffold for dual-lineage regeneration of osteochondral defect, Adv. Funct. Mater. 33 (2023), https://doi.org/10.1002/adfm.202304829.

[12] L. Zhang, W. Dai, C. Gao, W. Wei, R. Huang, X. Zhang, Y. Yu, X. Yang, Q. Cai, Multileveled hierarchical hydrogel with continuous biophysical and biochemical gradients for enhanced repair of full-thickness osteochondral defect, Adv. Mater. 35 (2023), https://doi.org/10.1002/adma.202209565.

[13] M. Hou, B. Tian, B. Bai, Z. Ci, Y. Liu, Y. Zhang, G. Zhou, Y. Cao, Dominant role of in situ native cartilage niche for determining the cartilage type regenerated by BMSCs, Bioact. Mater. 13 (2022) 149–160, https://doi.org/10.1016/j.bioactmat.2021.11.007.

[14] M.F. Pittenger, A.M. Mackay, S.C. Beck, R.K. Jaiswal, R. Douglas, J.D. Mosca, M. A. Moorman, D.W. Simonetti, S. Craig, D.R. Marshak, Multilineage potential of adult human mesenchymal stem cells, Science 284 (1999) 143–147, https://doi.org/10.1126/science.284.5411.143.

[15] H. Cho, J. Kim, S. Kim, Y.C. Jung, Y. Wang, B.J. Kang, K. Kim, Dual delivery of stem cells and insulin-like growth factor-1 in coacervate-embedded composite hydrogels for enhanced cartilage regeneration in osteochondral defects, J Control Release 327 (2020) 284–295, https://doi.org/10.1016/j.jconrel.2020.08.002.

[16] Y. Liu, Z. Yang, L. Wang, L. Sun, B.Y.S. Kim, W. Jiang, Y. Yuan, C. Liu, Spatiotemporal immunomodulation using biomimetic scaffold promotes endochondral ossification-mediated bone healing, Adv. Sci. 8 (2021) e2100143, https://doi.org/10.1002/advs.202100143.

[17] C. Xie, R. Liang, J. Ye, Z. Peng, H. Sun, Q. Zhu, X. Shen, Y. Hong, H. Wu, W. Sun, X. Yao, J. Li, S. Zhang, X. Zhang, H. Ouyang, High-efficient engineering of osteo-callus organoids for rapid bone regeneration within one month, Biomaterials 288 (2022) 121741, https://doi.org/10.1016/j.biomaterials.2022.121741.

[18] H. Zhang, Q. Li, X. Xu, S. Zhang, Y. Chen, T. Yuan, Z. Zeng, Y. Zhang, Z. Mei, S. Yan, L. Zhang, S. Wei, Functionalized microscaffold-hydrogel composites accelerating osteochondral repair through endochondral ossification, ACS Appl. Mater. Interfaces 14 (2022) 52599–52617, https://doi.org/10.1021/acsami.2c12694.

[19] K. Dai, S. Deng, Y. Yu, F. Zhu, J. Wang, C. Liu, Construction of developmentally inspired periosteum-like tissue for bone regeneration, Bone Res 10 (2022) 1, https://doi.org/10.1038/s41413-021-00166-w.

[20] T. Li, Z. Ma, Y. Zhang, Z. Yang, W. Li, D. Lu, Y. Liu, L. Qiang, T. Wang, Y. Ren, W. Wang, H. He, X. Zhou, Y. Mao, J. Zhu, J. Wang, X. Chen, K. Dai, Regeneration of humeral head using a 3D bioprinted anisotropic scaffold with dual modulation of endochondral ossification, Adv. Sci. 10 (2023) e2205059, https://doi.org/10.1002/advs.202205059.

[21] Y.A. Pei, S. Chen, M. Pei, The essential anti-angiogenic strategies in cartilage engineering and osteoarthritic cartilage repair, Cell. Mol. Life Sci. 79 (2022) 71, https://doi.org/10.1007/s00018-021-04105-0.

[22] J. Hao, B. Bai, Z. Ci, J. Tang, G. Hu, C. Dai, M. Yu, M. Li, W. Zhang, Y. Zhang, W. Ren, Y. Hua, G. Zhou, Large-sized bone defect repair by combining a decalcified bone matrix framework and bone regeneration units based on photo-crosslinkable osteogenic microgels, Bioact. Mater. 14 (2022) 97–109, https://doi.org/10.1016/j.bioactmat.2021.12.013.

[23] Z. Chen, W. Du, Y. Lv, Zonally stratified decalcified bone scaffold with different stiffness modified by fibrinogen for osteochondral regeneration of knee joint defect, ACS Biomater. Sci. Eng. 8 (2022) 5257–5272, https://doi.org/10.1021/acsbiomaterials.2c00813.

[24] Z. Man, X. Hu, Z. Liu, H. Huang, Q. Meng, X. Zhang, L. Dai, J. Zhang, X. Fu, X. Duan, C. Zhou, Y. Ao, Transplantation of allogenic chondrocytes with chitosan hydrogel-demineralized bone matrix hybrid scaffold to repair rabbit cartilage injury, Biomaterials 108 (2016) 157–167, https://doi.org/10.1016/j.biomaterials.2016.09.002.

[25] Q. Leng, Z. Liang, Y. Lv, Demineralized bone matrix scaffold modified with mRNA derived from osteogenically pre-differentiated MSCs improves bone repair, Mater Sci Eng C Mater Biol Appl 119 (2021) 111601, https://doi.org/10.1016/j.msec.2020.111601.

[26] Z. Liang, Y. Luo, Y. Lv, Mesenchymal stem cell-derived microvesicles mediate BMP2 gene delivery and enhance bone regeneration, J. Mater. Chem. B 8 (2020) 6378–6389, https://doi.org/10.1039/d0tb00422g.

[27] Z. Ci, Y. Zhang, Y. Wang, G. Wu, M. Hou, P. Zhang, L. Jia, B. Bai, Y. Cao, Y. Liu, G. Zhou, 3D cartilage regeneration with certain shape and mechanical strength based on engineered cartilage gel and decalcified bone matrix, Front. Cell Dev. Biol. 9 (2021) 638115, https://doi.org/10.3389/fcell.2021.638115.
[28] D. Fan, Y. Liu, Y. Wang, Q. Wang, H. Guo, Y. Cai, R. Song, X. Wang, W. Wang, 3D printing of bone and cartilage with polymer materials, Front. Pharmacol. 13 (2022) 1044726, https://doi.org/10.3389/fphar.2022.1044726.
[29] Q. Leng, L. Chen, Y. Lv, RNA-based scaffolds for bone regeneration: application and mechanisms of mRNA, miRNA and siRNA, Theranostics 10 (2020) 3190–3205, https://doi.org/10.7150/thno.42640.
[30] G.M. Keating, Axitinib: a review in advanced renal cell carcinoma, Drugs 75 (2015) 1903–1913, https://doi.org/10.1007/s40265-015-0483-x.
[31] Y. Huang, Y. Zhu, D. Cai, Q. Guo, J. Wang, L. Lei, X. Li, S. Shi, Penetrating-peptide-mediated non-invasive Axitinib delivery for anti-neovascularisation, J Control Release 347 (2022) 449–459, https://doi.org/10.1016/j.jconrel.2022.05.009.
[32] T.J. Ji, B. Feng, J. Shen, M. Zhang, Y.Q. Hu, A.X. Jiang, D.Q. Zhu, Y.W. Chen, W. Ji, Z. Zhang, H. Zhang, F. Li, An avascular niche created by axitinib-loaded PCL/collagen nanofibrous membrane stabilized subcutaneous chondrogenesis of mesenchymal stromal cells, Adv. Sci. 8 (2021) e2100351, https://doi.org/10.1002/advs.202100351.
[33] X. Ran, Q. Wang, Y. Sun, Q. Pan, H. Chen, W. Ren, Y. Huo, Y. Zhang, Y. Hua, G. Zhou, X. Wang, Dual microparticles programmed delivery system regulating stem cell-based cartilage regeneration by cartilage-specific matrix hydrogels, Compos. B Eng. (2024) 272, https://doi.org/10.1016/j.compositesb.2024.111221.
[34] T. Zhou, L. Yan, C. Xie, P. Li, L. Jiang, J. Fang, C. Zhao, F. Ren, K. Wang, Y. Wang, H. Zhang, T. Guo, X. Lu, A mussel-inspired persistent ROS-scavenging, electroactive, and osteoinductive scaffold based on electrochemical-driven in situ nanoassembly, Small 15 (2019) e1805440, https://doi.org/10.1002/smll.201805440.
[35] C.C. Ho, S.J. Ding, Novel SiO(2)/PDA hybrid coatings to promote osteoblast-like cell expression on titanium implants, J. Mater. Chem. B 3 (2015) 2698–2707, https://doi.org/10.1039/c4tb01841a.
[36] W. Chen, H. Miao, G. Meng, K. Huang, L. Kong, Z. Lin, X. Wang, X. Li, J. Li, X. Y. Liu, N. Lin, Polydopamine-induced multilevel engineering of regenerated silk fibroin fiber for photothermal conversion, Small 18 (2022) e2107196, https://doi.org/10.1002/smll.202107196.
[37] Y. Xiao, W. Wang, X. Tian, X. Tan, T. Yang, P. Gao, K. Xiong, Q. Tu, M. Wang, M. F. Maitz, N. Huang, G. Pan, Z. Yang, A Versatile Surface Bioengineering Strategy Based on Mussel-Inspired and Bioclickable Peptide Mimic, vol. 2020, Research (Wash D C), 2020 7236946, https://doi.org/10.34133/2020/7236946.
[38] G. Hu, Z. Liang, Z. Fan, M. Yu, Q. Pan, Y. Nan, W. Zhang, L. Wang, X. Wang, Y. Hua, G. Zhou, W. Ren, Construction of 3D-Bioprinted cartilage-mimicking substitute based on photo-crosslinkable Wharton's jelly bioinks for full-thickness articular cartilage defect repair, Mater Today Bio 21 (2023) 100695, https://doi.org/10.1016/j.mtbio.2023.100695.
[39] X. Zhao, S. Liu, L. Yildirimer, H. Zhao, R. Ding, H. Wang, W. Cui, D. Weitz, Injectable stem cell-laden photocrosslinkable microspheres fabricated using microfluidics for rapid generation of osteogenic tissue constructs, Adv. Funct. Mater. 26 (2016) 2809–2819, https://doi.org/10.1002/adfm.201504943.
[40] J. He, C. Chen, L. Chen, R. Cheng, J. Sun, X. Liu, L. Wang, C. Zhu, S. Hu, Y. Xue, J. Lu, H. Yang, W. Cui, Q. Shi, Honeycomb-Like Hydrogel Microspheres for 3D Bulk Construction of Tumor Models, vol. 2022, Research (Wash D C), 2022 9809763, https://doi.org/10.34133/2022/9809763.
[41] Z. Deng, W. Zhu, B. Lu, M. Li, D. Xu, A slotted decellularized osteochondral scaffold with layer-specific release of stem cell differentiation stimulators enhances cartilage and bone regeneration in osteochondral defects in a rabbit model, Am. J. Sports Med. 50 (2022) 3390–3405, https://doi.org/10.1177/03635465221114412.
[42] K. Liu, G.D. Zhou, W. Liu, W.J. Zhang, L. Cui, X. Liu, T.Y. Liu, Y. Cao, The dependence of in vivo stable ectopic chondrogenesis by human mesenchymal stem cells on chondrogenic differentiation in vitro, Biomaterials 29 (2008) 2183–2192, https://doi.org/10.1016/j.biomaterials.2008.01.021.
[43] P. Dy, W. Wang, P. Bhattaram, Q. Wang, L. Wang, R.T. Ballock, V. Lefebvre, Sox9 directs hypertrophic maturation and blocks osteoblast differentiation of growth plate chondrocytes, Dev. Cell 22 (2012) 597–609, https://doi.org/10.1016/j.devcel.2011.12.024.
[44] R.M. Raftery, A.G. Gonzalez Vazquez, G. Chen, F.J. O'Brien, Activation of the SOX-5, SOX-6, and SOX-9 trio of transcription factors using a gene-activated scaffold stimulates mesenchymal stromal cell chondrogenesis and inhibits endochondral ossification, Adv Healthc Mater 9 (2020) e1901827, https://doi.org/10.1002/adhm.201901827.
[45] T.J. Levingstone, A. Matsiko, G.R. Dickson, F.J. O'Brien, J.P. Gleeson, A biomimetic multi-layered collagen-based scaffold for osteochondral repair, Acta Biomater. 10 (2014) 1996–2004, https://doi.org/10.1016/j.actbio.2014.01.005.
[46] Y. Zhu, L. Kong, F. Farhadi, W. Xia, J. Chang, Y. He, H. Li, An injectable continuous stratified structurally and functionally biomimetic construct for enhancing osteochondral regeneration, Biomaterials 192 (2019) 149–158, https://doi.org/10.1016/j.biomaterials.2018.11.017.
[47] C. Erggelet, K. Neumann, M. Endres, K. Haberstroh, M. Sittinger, C. Kaps, Regeneration of ovine articular cartilage defects by cell-free polymer-based implants, Biomaterials 28 (2007) 5570–5580, https://doi.org/10.1016/j.biomaterials.2007.09.005.
[48] J. Liu, Y. Lu, F. Xing, J. Liang, Q. Wang, Y. Fan, X. Zhang, Cell-free scaffolds functionalized with bionic cartilage acellular matrix microspheres to enhance the microfracture treatment of articular cartilage defects, J. Mater. Chem. B 9 (2021) 1686–1697, https://doi.org/10.1039/d0tb02616f.